J|A|C|S
ARTICLES
Published on Web 10/24/2006

Order−Disorder Transition Coupled with Magnetic Bistability in the Ferricinium Salt of a Radical Nickel Dithiolene Complex

Olivier Jeannin,[†] Rodolphe Clérac,[‡] and Marc Fourmigué*[,†,§]

Contribution from the Laboratoire CIMMA, UMR 6200 CNRS-Université d'Angers, UFR Sciences, 2 Bd Lavoisier, 49045 Angers, France, Centre de Recherches P. Pascal (CRPP-UPR CNRS 8641), Equipe M³, 115 Avenue du Dr. A. Schweitzer, 33600 Pessac, France, and Sciences Chimiques de Rennes, UMR 6226 CNRS-Université Rennes 1, Equipe MaCSE, Bât 10C, Campus de Beaulieu, 35042 Rennes Cedex, France

Received July 7, 2006; E-mail: marc.fourmigue@univ-rennes1.fr

Abstract: The ferricinium salt of the anionic, $S = {}^1/_2$, dithiolene complex $[Ni(tfadt)_2]^-$ (where tfadt is the asymmetrically substituted 2-(trifluoromethyl)acrylonitrile-1,2-dithiolate) crystallizes at room temperature (rt) into uniform chains of dithiolene complexes, separated by ferricinium cations. Both ionic entities are characterized by disorder affecting one CF_3 and one Cp moiety. Above 250 K, this compound displays a Curie-type behavior. At lower temperatures, two first-order transitions around 249 and 137 K are revealed by susceptibility measurements and the observation of hysteresis effects. Crystal structure determinations performed at 230 and 120 K show that the high-temperature transition is associated with an ordering of the CF_3 and Cp groups together with a dimerization of the anionic stacks that thus induces a drop of the susceptibility. The second, low-temperature transition leads to a tetramerization of these nickel dithiolene stacks now in a complete diamagnetic state while the remaining susceptibility originates from the sole ferricinium contribution. The first order character of the 249 K transition with its associated bistable behavior is likely correlated with the structural order−disorder transition, an original behavior in this class of materials where bistability is most often associated with a strengthening of interstack intermolecular interactions (hydrogen bonding, $\pi-\pi$ interactions ...).

Introduction

Order−Disorder Transitions (ODT) are currently a very broad research topic in condensed matter physics covering various materials, such as, to name a few, (i) diblock copolymers,[1] (ii) hydrogen-bonded lattices with proton ordering processes (KCP, squaric acid, ...),[2,3] (iii) disordered guest molecules in crystalline inclusion compounds,[4] or (iv) Langmuir−Blodgett films or self-assembled monolayers.[5] Such order−disorder transitions also strongly influence the electronic properties of crystalline molecular materials based on *radical* molecules and blessed with conducting or magnetic properties. As characteristic examples among organic superconductors, we can cite the ordering of tetrahedral anions (such as X: ClO_4^- or ReO_4^-) on centrosymmetric sites in the Bechgaard salts $(TMTSF)_2X$ (TMTSF: TetraMethylTetraSelenaFulvalene)[6] or the ordering of the ethylenic bridges of BEDT-TTF (BEDT-TTF: Bis(EthyleneDiThio)TetraThiaFulvalene) molecules in BEDT-TTF salts,[7] which eventually controls their superconducting transition.[8] Similarly, C_{60}^{x-} orientational ordering plays a key role in fulleride structure−property relationships.[9] Insulating magnetic materials are also concerned with such transitions,[10,11] as in a few iron complexes where the spin crossover phenomenon is sometimes associated with an order−disorder transition involving the counterions,[12] including solvent molecules[13] and even the ligand coordinating the metal atom.[14] It was suggested that modifications of the ligand field strength upon ligand ordering,

† CIMMA, Angers.
‡ CRPP, Bordeaux.
§ CNRS-Université de Rennes 1.

(1) (a) Leibler, L. *Macromolecules* **1980**, *13*, 1602. (b) Hashimoto, T.; Kimishima, K.; Hasegawa, H. *Macromolecules* **1991**, *24*, 5704.
(2) For example, see: Okishiro, K.; Yamamuro, O.; Matsuo, T.; Nishikiori, S.; Iwamoto, T. *J. Phys. Chem.* **1996**, *100*, 18546.
(3) Levin, A. A.; Dolin, S. P. *J. Phys. Chem.* **1996**, *100*, 6258
(4) Prout, K.; Heyes, S. J.; Dobson, C. M.; McDaid, A.; Maris, T.; Muller, M.; Seaman, M. J. *Chem. Mater.* **2000**, *12*, 3561 and references therein.
(5) Gao, W.; Dickinson, L.; Grozinger, C.; Morin, F. G.; Reven, L. *Langmuir* **1997**, *13*, 115
(6) (a) Pouget, J.-P.; Ravy, S. *J. Phys. I* **1996**, *6*, 1501. (b) Ravy, S. *Chem. Rev.* **2004**, *104*, 5609.
(7) (a) Schlueter, J. A.; Williams, J. M.; Geiser, U.; Dudek, J. D.; Kelly, M. E.; Sirchio, S. A.; Carlson, K. D.; Naumann, D.; Roy, T.; Campana, C. F. *Adv. Mater.* **1995**, *7*, 634. (b) Ward, B. H.; Schlueter, J. A.; Geiser, U.; Wang, H. H.; Morales, E.; Parakka, J. P.; Thomas, S. Y.; Willams, J. M.; Nixon, P. G.; Winter, R. W.; Gard, G. L.; Koo, H.-J.; Whangbo, M.-H. *Chem. Mater.* **2000**, *12*, 343. (c) Davidson, A.; Boubekeur, K.; Pénicaud, A.; Auban, P.; Lenoir, C.; Batail, P.; Hervé G. *J. Chem. Soc., Chem. Commun.* **1989**, 1373. (d) Deluzet, A.; Batail, P.; Misaki, Y.; Auban-Senzier, P.; Canadell, E. *Adv. Mater.* **2000**, *12*, 436.
(8) (a) Whangbo, M.-H.; Williams, J. M.; Schultz, A. J.; Emge, T. J.; Beno, M. A. *J. Am. Chem. Soc.* **1987**, *109*, 90. (b) Whangbo, M.-H.; Jung, D.; Ren, J.; Evain, M.; Novoa, J. J.; Mota, F.; Alvarez, S.; Williams, J. M.; Beno, M. A.; Kini, M. A.; Wang, H. H.; Ferraro, J. R. In *The Physics and Chemistry of Organic Superconductors*; Saito, G., Kagoshima, S., Eds.; Springer: Heidelberg, Germany, 1990; p 262.
(9) (a) Zhou, O.; Cox, D. E. *J. Phys. Chem. Solids* **1992**, *53*, 1373. (b) Dahlke, P.; Rosseinsky, M. J. *Chem. Mater.* **2002**, *14*, 1285.
(10) Liu, H.-L.; Chou, L.-K.; Abboud, K. A.; Ward, B. H.; Fanucci, G. E.; Granroth, G. E.; Canadell, E.; Meisel, M. W.; Talham, D. R.; Tanner, D. B. *Chem. Mater.* **1997**, *9*, 1865
(11) (a) Clérac, R.; Fourmigué, M.; Gaultier, J.; Barrans, Y.; Albouy, P. A.; Coulon, C. *Eur. Phys. J. B* **1999**, *9*, 431. (b) Clérac, R.; Fourmigué, M.; Gaultier, J.; Barrans, Y.; Albouy, P. A.; Coulon, C. *Eur. Phys. J. B* **1999**, *9*, 445.

Chart 1

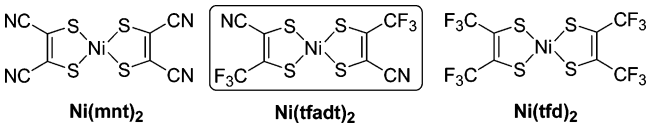

combined with the cooperative interactions due to the ordering of a counteranion, provided an intrinsic impulse for the initiation of the spin crossover and, most importantly perhaps, to afford broad hysteresis loops. Therefore, a *strong coupling* between an order−disorder transition *and* an electronic transition, as, for example, in a "spin transition", can appear as a useful tool for the elaboration of molecular switches with potential applications in molecular electronics[15] for memory or sensing applications.[16]

Recently, paramagnetic metal-bis-dithiolene complexes such as $[Ni(mnt)_2]^{-\bullet}$ salts (Chart 1, where mnt^{2-} is maleonitriledithiolate or 1,2-dicyanoethene-1,2-dithiolate) were shown to exhibit abrupt paramagnetic−diamagnetic transitions[17] related to those described in neutral radical systems such as 1,3,5-trithia-2,4,6-triazapentalenyl (TTTA)[18,19] or dithiazolyl radicals.[20] However, the absence of hysteresis in those salts, an essential feature for many applications, has urged for example the elaboration of $[Ni(mnt)_2]^{-\bullet}$ salts with the counterion having hydrogen bonding capability,[21] in order to eventually increase the intermolecular cooperativity held responsible for wide hysteresis in spin-crossover systems and TTTA radical systems. We postulated that the purposeful introduction of disordered groups in such metal dithiolene salts with an opposite *softening* of the crystal phases could offer an original and efficient alternative for favoring a bistable character by coupling the magnetic properties to an order−disorder transition. In that respect, we have recently reported the synthesis of an original asymmetrically substituted dithiolate ligand, the 2-(trifluoromethyl)acrylonitrile-1,2-dithiolate abbreviated as tfadt, which incorporates, besides the nitrile moiety found in the mnt dithiolate, a trifluoromethyl group characteristic of the tfd dithiolate ligand (Chart 1).[22] This CF_3 group often exhibits conformational disorder with rotation around the $C-C(F_3)$ axis. The latter is a consequence of the weak van der Waals interactions of fluorine atoms, leading to a segregation of fluorinated moieties in the solid state.[23]

Scheme 1

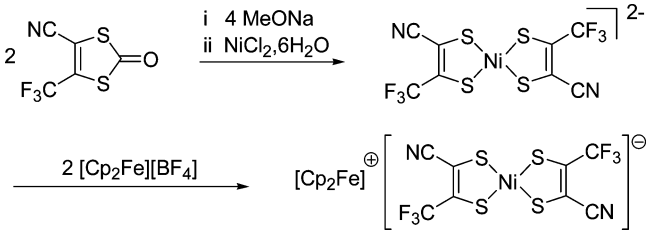

While the reported $n\text{-}Bu_4N^+$ and PPh_4^+ salts of $[Ni(tfadt)_2]^{-\bullet}$ exhibit Curie-type behavior between 2 and 300 K,[22] we have found and describe here that its ferricinium salt has a rich phase diagram based on the room-temperature (rt) disorder of both one $-CF_3$ group and one Cp ring. We analyze here the temperature dependence of its structural and magnetic properties and investigate the correlation between the order−disorder/structural transitions and the magnetic susceptibility.

Results

Synthesis. The preparation of the $[Ni(tfadt)_2]^{-\bullet}$ nickel complex as $n\text{-}Bu_4N^+$ or PPh_4^+ salt has been recently described[22] and involves the reaction of 4-cyano-5-trifluoromethyl-1,3-dithiole-2-one with successively (i) MeONa to generate the dithiolate, (ii) $NiCl_2(H_2O)_6$ to form the dianionic complex $[Ni(tfadt)_2]^{2-}$, (iii) $n\text{-}Bu_4NBr$ or PPh_4Br to precipitate the dianion salt, (iv) 1 equiv of $[Cp_2Fe][BF_4]$ to oxidize to the monoanioinic $[Ni(tfadt)_2]^{-\bullet}$ species directly as $n\text{-}Bu_4N^+$ or PPh_4^+ salt. Since ferricinium was already used for the oxidation step, we decided to prepare $[Cp_2Fe][Ni(tfadt)_2]$ by the same procedure starting from 4-cyano-5-trifluoromethyl-1,3-dithiole-2-one and using 2 equiv of $[Cp_2Fe][BF_4]$ to work both as an oxidant and for the metathesis, as shown in Scheme 1.

Room-Temperature Structural Arrangement. The best crystals of $[Cp_2Fe][Ni(tfadt)_2]$ were obtained by slow evaporation of a CH_2Cl_2 solution. It crystallizes in the monoclinic system, space group $C2/m$, with both cation and anion located on the mirror plane. This rt phase will be described as phase **A** in the following discussion. The whole dithiolene complex lies

(12) (a) König, E.; Ritter, G.; Kulshreshtha, S. K.; Nelson, S. M. *Inorg. Chem.* **1982**, *21*, 3022. (b) Fleisch, J.; Gütlich, P.; Hasselbach, K. M.; Müller, W. *Inorg. Chem.* **1976**, *15*, 958. (c) Weihl, E. *Acta Crystallogr., Sect. B* **1993**, *49*, 289. (d) Breuning, E.; Ruben, M.; Lehn, J.-M.; Renz, F.; Garcia, Y.; Ksenofontov, V.; Gütlich, P.; Wegelius, E.; Rissanen, K. *Angew. Chem., Int. Ed.* **2000**, *39*, 2504. (e) Holland, J. M.; McAllister, J. A.; Lu, Z.; Kilner, C. A.; Thornton-Pett, M.; Halcrow, M. A. *Chem. Commun.* **2001**, *577*. (f) Matouzenko, G. S.; Molnar, G.; Bréfuel, N.; Perrin, M.; Bousseksou, A.; Borshch, S. A. *Chem. Mater.* **2003**, *15*, 550.

(13) (a) Mikami, M.; Konno, M. Saito, Y. *Chem. Phys. Lett.* **1979**, *63*, 566. (b) Katz, B. A.; Strouse, C. E. *J. Am. Chem. Soc.* **1979**, *101*, 6214. (c) Mikami, M.; Konno, M.; Saito, Y. *Acta Crystallogr., Sect. B* **1980**, *36*, 275. (d) König, E.; Ritter, G.; Kulshreshtha, S. K.; Waigel, J.; Sacconi, L. *Inorg. Chem.* **1984**, *23*, 1241. (e) Weihl, L.; Kiel, G.; Köhler, C. P.; Spiering, H.; Gütlich, P. *Inorg. Chem.* **1986**, *25*, 1565. (f) Conti, A. J.; Chadha, R. K.; Sena, K. M.; Rheingold, A. L.; Hendrickson, D. N. *Inorg. Chem.* **1993**, *32*, 2670. (g) Conti, A. J.; Kaji, K.; Nagano, Y.; Sena, K. M.; Yumoto, Y.; Chadha, R. K.; Rheingold, A. L.; Sorai, M.; Hendrickson, D. N. *Inorg. Chem.* **1993**, *32*, 2681. (h) Wu, C.-C.; Jung, J.; Gantzel, P. K.; Gütlich, P.; Hendrickson, D. N. *Inorg. Chem.* **1997**, *36*, 5339

(14) Matouzenko, G. S.; Bousseksou, A.; Borshch, S. A.; Perrin, M.; Zein, S.; Salmon, L.; Molnar, G.; Lecocq, S. *Inorg. Chem.* **2004**, *43*, 227

(15) (a) Roubeau, O.; Colin, A.; Schmitt, V.; Clérac, R. *Angew. Chem., Int. Ed.* **2004**, *43*, 3283. (b) Carroll, R. L.; Gorman, C. B. *Angew. Chem., Int. Ed.* **2002**, *41*, 4378. (c) Bousseksou, A.; Molnar, G.; Matouzenko, G. *Eur. J. Inorg. Chem.* **2004**, 4353. (d) de Silva, A. P.; McClenaghan, N. D. *Chem.—Eur. J.* **2004**, *10*, 574. (e) Pease, A. R.; Jeppesen, J. O.; Stoddart, J. F.; Luo, Y.; Collier, C. P.; Heath, J. R. *Acc. Chem. Res.* **2001**, *34*, 433.

(16) (a) de Silva, A. P.; Gunaratne, H. Q. N.; Gunnlaugsson, T.; Huxley, A. J. M.; McCoy, C. P.; Rademacher, J. T.; Rice, T. E. *Chem. Rev.* **1997**, *97*, 1515. (b) Photochromism: Memories and Switches Special Issue. *Chem. Rev.* **2000**, *100*, 1683. (d) Sato, O. *Acc. Chem. Res.* **2003**, *36*, 692. Dei, A.; Gatteschi, D.; Sangregorio, C.; Sorace, L. *Acc. Chem. Res.* **2004**, *37*, 827.

(17) (a) Ren, X.; Meng, Q.; Song, Y.; Hu, C.; Lu, C.; Chen, C.; Xue, Z. *Inorg. Chem.* **2002**, *41*, 5931. (b) Ren, X. M.; Okudera, H.; Kremer, R. K.; Song, Y.; He, C.; Meng, Q. J.; Wu, P. H. *Inorg. Chem.* **2004**, *43*, 2569. (c) Ren, X.; Meng, Q.; Song, Y.; Lu, C.; Hu, C. *Inorg. Chem.* **2002**, *41*, 5686.

(18) (a) Fujita, W.; Awaga, K. *Science* **1999**, *286*, 261. (b) Fujita, W.; Awaga, K.; Kondo, R.; Kagoshima, S. *J. Am. Chem. Soc.* **2006**, *128*, 6016.

(19) (a) Brusso, J. L.; Clements, O. P.; Haddon, R. C.; Itkis, M. E.; Leitch, A. A.; Oakley, R. T.; Reed, R. W.; Richardson, J. F. *J. Am. Chem. Soc.* **2004**, *126*, 8256. (b) Barclay, T. M.; Cordes, A. W.; George, N. A.; Haddon, R. C.; Itkis, M. E.; Mashuta, M. S.; Oakley, R. T.; Patenaude, G. W.; Reed, R. E. W.; Richardson, J. F.; Zhang, H. *J. Am. Chem. Soc.* **1998**, *120*, 352. (c) Brusso, J. L.; Clements, O. P.; Haddon, R. C.; Itkis, M. E.; Leitch, A. A.; Oakley, R. T.; Reed, R. W.; Richardson, J. F. *J. Am. Chem. Soc.* **2004**, *126*, 14692.

(20) (a) Alberola, A.; Collis, R. J.; Humphrey, S. M.; Less, R. J.; Rawson, J. M. *Inorg. Chem.* **2006**, *45*, 1903. (b) Banister, A. J.; Bricklebank, N.; Lavender, I.; Rawson, J. M.; Gregory, C. I.; Tanner, B. K.; Clegg, W.; Elsegood, M. R. J.; Palacio, F. *Angew. Chem., Int. Ed. Eng.* **1996**, *35*, 2533.

(21) Ren, X. M.; Nishihara, S.; Akutagawa, T.; Noro, S.; Nakamura, T. *Inorg. Chem.* **2006**, *45*, 2229.

(22) Jeannin, O.; Delaunay, J.; Barrière, F.; Fourmigué, M. *Inorg. Chem* **2005**, *44*, 9763

(23) Dautel, O. J.; Fourmigué, M. *J. Org. Chem.* **2000**, *65*, 6479. (b) Dautel, O. J.; Fourmigué, M. *Inorg. Chem.* **2001**, *40*, 2083. (c) Dautel, O. J.; Fourmigué M.; Canadell, E.; Auban-Senzier, P. *Adv. Funct. Mater.* **2002**, *12*, 693. (d) Jeannin, O.; Fourmigué M. *Chem.—Eur. J.* **2006**, *12*, 2994.

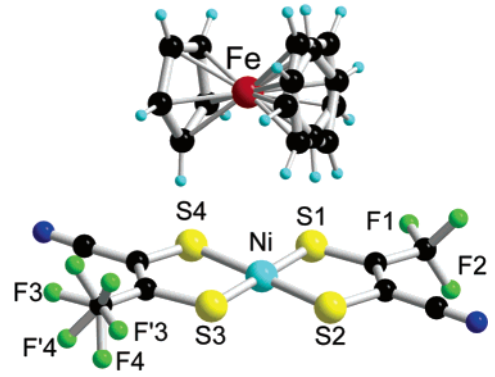

Figure 1. Disorder model of one of the Cp rings (top) and one CF_3 group (bottom) in $[Cp_2Fe][Ni(tfadt)_2]$, at rt. The fluorine atoms F3, F′3, and F1 are located in the mirror plane containing the whole dithiolene complex.

flat on the mirror plane except some fluorine atoms of the CF_3 groups. Furthermore, one of the two CF_3 groups is disordered on two positions related to each other by a $\pi/6$ rotation around the C−C(F_3) axis (Figure 1). For the $[Cp_2Fe]^+$ cation, the mirror plane includes the metal center and one carbon atom of each Cp ring while one of the Cp rings is also disordered on two positions related by a $\pi/5$ rotation (Figure 1).

In the solid state (Figure 2), the dithiolene complexes stack along the *b* axis in a zigzag fashion. These anionic columns are separated from each other in the *a* direction by dyads of ferricinium cations filling pockets between the dithiolene stacks. Within these dyads, the metallocene moieties are organized on top of each other with the disordered Cp rings of both complexes facing each other in a decaled $\pi-\pi$ overlap with an intermolecular plane-to-plane distance of 3.375(5) Å.

This original combination of stacked dithiolene complexes and metallocenium dyads leads to the formation of hybrid layers parallel to the (*a*,*b*) plane, which reproduce by translation along the *c* direction. The interface between those layers is essentially formed by CF_3 and Cp moieties pointing toward each other, most probably a soft interaction that allows us to describe these salts as layered compounds. It is also very important to note that the chains of dithiolene complexes running along *b* are *uniform* stacks, (i) with a single overlap pattern between the radical anions (Figure 3a), (ii) characterized by a large interplanar distance ($b/2 = 3.874$ Å) and by the shortest intermolecular Ni···S distance at 3.90 Å and shortest S···S distance at 4.21 Å. Note that the uniform spin chains of dithiolene radical anions are also fully isolated from each other in the layers by the metallocenium cations but also between layers through the nonbonding soft fluorine−fluorine interface. This confined character and absence of *direct* interchain coupling might have an important consequence on the magnetic behavior of the chains as seen below.

Overview of the Physical Properties. These large intermolecular distances, combined with the negligible overlap interaction energy between complexes ($\beta = 0.0038$ eV, $\beta/k_B = 44$ K) determined from Extended Hückel calculations, indicate that, from a magnetic point of view, the radical species are essentially isolated from each other. Indeed, the χT product is constant around rt (Figure 4) confirming the presence of noninteracting spins. This Curie-type behavior with $C = 1.0$ cm^3 K mol^{-1} results from the addition of the contributions of the two $S = {}^1/_2$ paramagnetic species: the $[Ni(tfadt)_2]^{-\bullet}$ (with $g = 2$ and thus $C \approx 0.375$ cm^3 K mol^{-1}) and the ferricinium cation. The latter

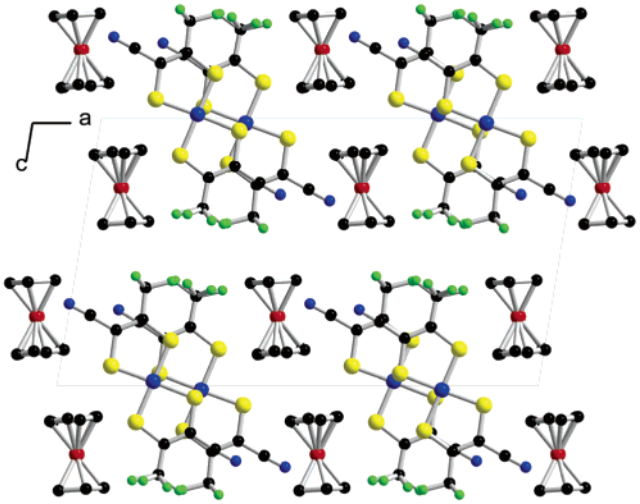

Figure 2. Projection view along *b* of the unit cell of $[Cp_2Fe][Ni(tfadt)_2]$ at rt.

is known to exhibit strong deviations from the spin-only value with Curie constant values between 0.66 and 0.84 cm^3 K mol^{-1}, depending on the nature of the counterion while a χT value of 0.67 cm^3 K mol^{-1} is reported in the solution.[24]

As shown in Figure 4, the temperature dependence of χT also exhibits two anomalies below room temperature that strongly suggest a modification of the magnetic interactions in the material probably correlated to structural transitions. While between 243 and 254 K, a strong discontinuity associated to a thermal hysteresis is observed, and a second weaker hysteresis is detected around 137 K. As shown in Figure 5, the Differential Scanning Calorimetry (DSC) thermograms confirm the presence of two successive transitions with large enthalpy changes exactly at the temperatures where susceptibility anomalies were also identified (Table 1). Note that the ΔS values exceed the spin-only value for a paramagnetic−diamagnetic transition (R ln 2 = 5.76 J K^{-1} mol^{-1}),[25] indicating that degrees of freedom of the lattice are also involved in the transitions, as indeed observed in the low-temperature X-ray crystal structures (see below).

249 K Order−Disorder Transition. A detailed χT vs T view of the first transition is shown in Figure 6a emphasizing the first-order character of the transition with a well-defined hysteresis ($\Delta T \approx 11$ K). When lowering the temperature, the susceptibility abruptly decreases at 243 K to reach a pseudo-plateau in the χT product at 0.65 cm^3 K mol^{-1} that corresponds to the progressive disappearance of the contribution of the $S = 1/2$ dithiolene complex.

To rationalize this behavior, data collections were performed on the same crystal above and then below the phase transition, namely at 230 K. Note that the cooling process to go through the transition needed to be very slow since, otherwise, the mechanical stress induced by the structural transition led to a fragmentation of the crystal. Using a cooling rate of −1 K/h (−0.017 K/min), we succeeded to collect good quality data on the very same single crystal at 293 and 230 K. The structure of the phase at 230 K, called **B** in the following, was solved in the triclinic system, space group $P\bar{1}$ with both ferricinium and dithiolene complexes in a general position in the unit cell. As a consequence, the dithiolene complex is not fully planar

(24) Hendrickson, D. N.; Sohn, Y. S.; Gray, H. B. *Inorg. Chem.* **1971**, *10*, 1559.
(25) We thank one of the reviewers for suggesting this comparison.

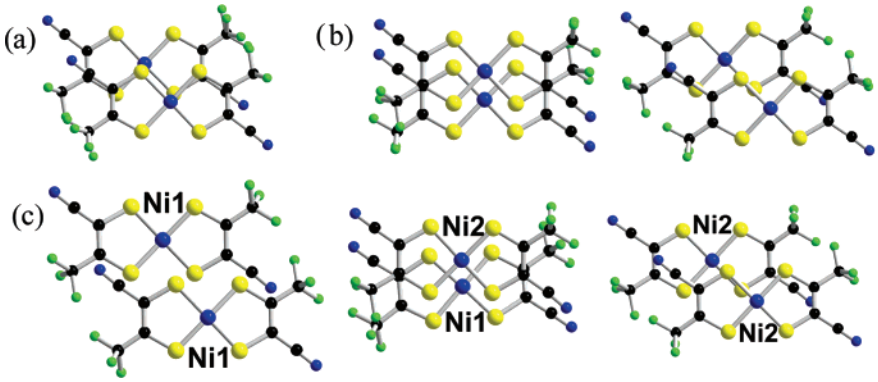

Figure 3. Overlap patterns between $[Ni(tfadt)_2]^{-\bullet}$ species in $[Cp_2Fe][Ni(tfadt)_2]$, (a) within the uniform chain in the **A** phase at rt, (b) within the alternated chains in the **B** phase at 230 K, (c) within the tetramerized chain in the **C** phase at 120 K (see text).

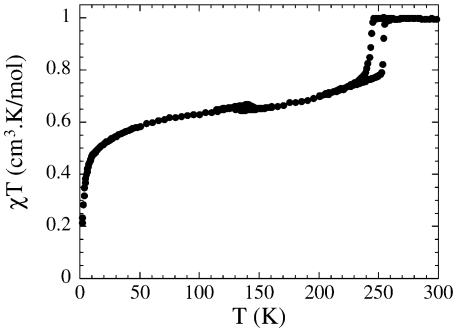

Figure 4. Plot of χT vs T (with $\chi = M/H$) in the 1.85−300 K range at 1000 Oe with a 0.4 K/min sweep rate.

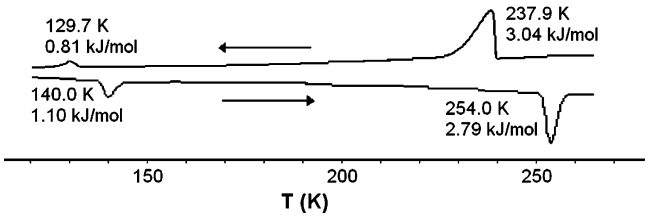

Figure 5. DSC thermogram of $[Cp_2Fe][Ni(tfadt)_2]$, with indication of the associated enthalpies (ΔH). Cooling rate 10 K/min, warming rate 5 K/min.

Table 1. Transition Temperatures (T_t), Transition Enthalpies (ΔH_t), and Transition Entropies (ΔS_t) for the Two First-Order Transitions in $[Cp_2Fe][Ni(tfadt)_2]$

T_t (K)	ΔH_t (kJ mol^{-1})	ΔS_t (J K^{-1} mol^{-1})
245.90	2.90	11.87
134.85	0.95	7.06

anymore but adopts a slight deformation toward a tetrahedron with an angle between the two metallacycle mean planes of 5.6(1)°. Furthermore, the disorder observed in the rt structure on one CF_3 group and one Cp ring has fully disappeared at the transition. The two Cp rings of the ferricinium are now almost eclipsed while the two CF_3 groups are ordered and adopt different conformations with the fluorine atom located in the molecular plane (in bold in Scheme 2) pointing toward the neighboring CN group in one CF_3 group, pointing toward the sulfur atom in the other CF_3 group.

A projection view along the *a* axis (Figure 7) allows for a preliminary comparison with the rt structure shown in Figure 2 showing apparently limited differences. However, as shown in Figure 8, striking modifications of the dithiolene stack are observed.

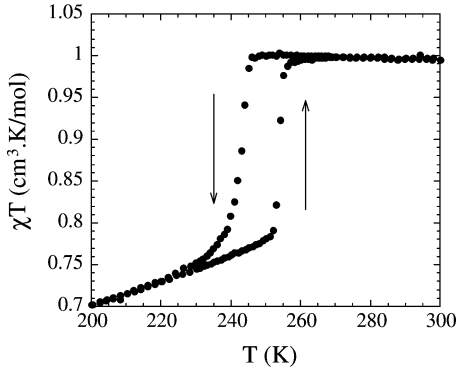

Figure 6. Details of the χT vs T plot between 200 and 300 K for **1** at 10000 Oe with a 0.4 K/min sweep rate.

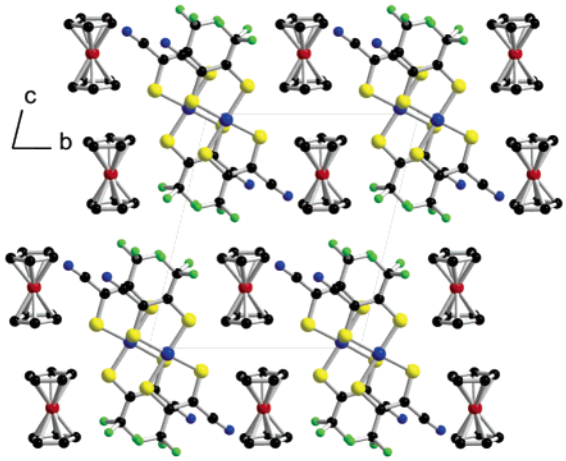

Figure 7. Projection view along *a* of the unit cell of $[Cp_2Fe][Ni(tfadt)_2]$ below the first transition, at 230 K (**B** phase).

Scheme 2

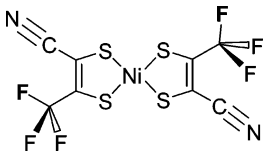

The uniform chain with the large interplanar distance found at rt (3.874 Å) is now strongly dimerized, with much shorter plane-to-plane distances, at 3.705(8) Å (Ni···Ni 3.919 Å) and 3.741(8) Å (Ni···Ni 5.003 Å) for the intra- and interdyad interactions, respectively. The intradyad overlap is characterized by an almost eclipsed configuration (Figure 3b), with a lateral

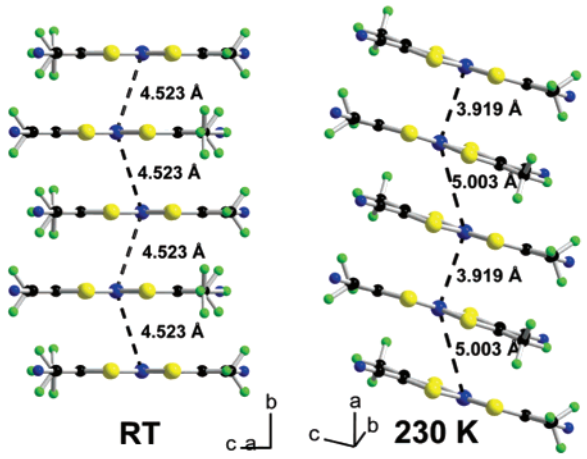

Figure 8. A view of the dithiolene stacks in $[Cp_2Fe][Ni(tfadt)_2]$. (Left) At 293 K, **A** phase and (right) at 230 K, **B** phase, showing the dimerization of the $[Ni(tfadt)_2]^{-\bullet}$ chain in the **B** phase. The Ni···Ni distances are marked with dashed lines.

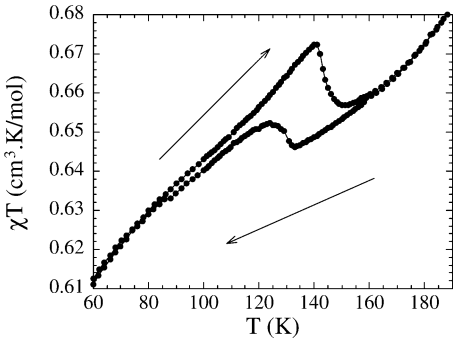

Figure 9. Detail of the temperature dependence of χT between 60 and 180 K at 10000 Oe with a 0.4 K/min sweep rate.

offset of 1.16(8) Å while the interdyad overlap is characterized by a large lateral offset (2.33(7) Å). As a consequence, two different β overlap interaction energies are now to be considered to describe the magnetic interaction within the chains; they amount to 0.25 and 0.15 eV for the intra- and interdyad overlaps, respectively, to be compared with the 0.004 eV value determined in the rt regime. In such alternated magnetic chains, two J and αJ values, with $0 < \alpha < 1$, are to be considered.[26] Since the ratio of J values behaves as the ratio of β^2 values, an α value of 0.36 can be anticipated, characteristic of a strong alternation of the magnetic chains. Thus, along the **A** → **B** transition, the uniform chain with weak intermolecular interactions transforms into an alternated chain with stronger interactions inducing naturally this sudden decrease of the χT product from 1 to 0.75 cm^3 K mol^{-1}. Further temperature lowering leads to a smooth decrease of the χT product, a behavior normally associated with alternated spin chain systems characterized indeed by an activated susceptibility and a singlet ground state. Since this first-order transition is also characterized by a simultaneous ordering of the disordered CF_3 and Cp moieties, a question then arises about the exact nature of the driving forces, of structural or electronic origin, that induces the phase transition (vide infra).

137 K Tetramerization Transition. A detailed χT vs T view of the second transition identified around 137 K is shown in Figure 9. Upon cooling from the alternated **B** phase, a sudden small susceptibility increase is observed at 145 K, while, upon warming back, another kink is found at 129 K, affording here a 16 K hysteresis. To get further insight into the nature of the low-temperature phase, a third data collection at 120 K was attempted. However, crossing this second anomaly was even more difficult since the crystal often broke into parts at this transition, a probable consequence of strong mechanical stress already experienced at the first transition.[27] We finally succeed to collect X-ray data at 120 K, after a slow cooling at 1 K/h (−0.017 K/min), (see Experimental Section).

Note that the phase transitions observed here are not limited to one single crystal which would, by chance, exhibit such a rich behavior. Several crystals were investigated, which all showed the same transitions at the same temperatures. Our confidence is also based on the precise correlation between the temperatures deduced from these single-crystal X-ray diffraction studies and the temperatures deduced from the DSC and magnetic susceptibility measurements that were performed on several milligrams of this salt.

At 120 K, a novel third phase (**C**) was identified that crystallizes in the triclinic system, space group $P\bar{1}$, with now two crystallographically independent ferricinium cations and two crystallographically independent $[Ni(tfadt)_2]^{-\bullet}$ anions, all of them free of disordered groups. Note however that, in one of the ferricinium cations, the Cp rings are perfectly eclipsed, while,

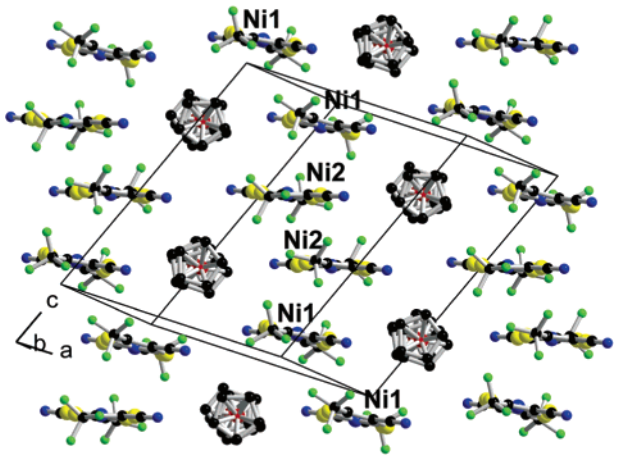

Figure 10. A view of the **C** phase at 120 K showing the organization within the dithiolene stacks.

Table 2. Structural Characteristics (in Å) and Overlap Energies (in eV) of the Overlap Patterns at 230 K (phase **B**) and 120 K (Phase **C**)

interaction	interplane distance	Ni···Ni distance	lateral shift	β (eV)
Ni−Ni @ 230 K (**B**)	3.705(8)	3.919(2)	1.16	0.25
Ni−Ni @ 230 K (**B**)	3.741(8)	5.003(2)	3.36	0.15
Ni1−Ni1 @ 120 K (**C**)	3.735(5)	5.711(3)	4.32	0.11
Ni1−Ni2 @ 120 K (**C**)	*a*	3.899(3)	1.19	0.27
Ni2−Ni2 @ 120 K (**C**)	3.588(3)	4.785(3)	3.17	0.18

[a] The dithiolene complexes based on Ni1 and Ni2 are not coplanar.

(26) Kahn, O. In *Molecular Magnetism*; VCH: Weinheim, 1993.

(27) Some readers may be concerned with the quality of the diffraction data for the phases **B** and **C**. The overall quality of X-ray data collected on crystals that undergo one or even two first-order phase transitions cannot be compared with that of those obtained at low temperatures in the absence of phase transitions. The only way to collect data on the different phases was by having the crystals undergo phase transitions on the diffractometer starting from the room temperature phase. Though reversible, the phase transitions cannot be expected to leave the crystals unaffected. See, for example: Grepioni, F.; Cojazzi, G.; Draper, S. M.; Scully, N.; Braga, D. *Organometallics* **1998**, *17*, 296.

in the other one, the Cp rings are rotated by 6° relative to each other. Differences of $-CF_3$ orientation are also observed between the two independent $[Ni(tfadt)_2]^{-\bullet}$ complexes, one of them with the model found in the **B** phase and shown in Scheme 2, while the other complex exhibits $-CF_3$ moieties without any fluorine atoms in the mean molecular plane. Furthermore, the dithiolene complexes are not fully planar and exhibit a slight distortion toward a tetrahedron with angles between the metallacycle mean planes of 5.1(1)° and 3.9(1)° around Ni1 and Ni2, respectively. These structural differences justify the presence of two crystallographically independent molecules.

In the solid state, the overall layered structure described in phase **A** is preserved, but the details of the organization within each layer differ markedly in the **C** phase from what was observed in phases **A** and **B**. Indeed, as shown in Figure 10, the stacks of nickel dithiolene complexes are now formed by inversion-centered Ni1−Ni1 dyads alternating with inversion-centered Ni2−Ni2 dyads. Three different magnetic interactions thus need to be considered, related to the Ni1−Ni1, Ni1−Ni2, and Ni2−Ni2 overlap patterns (Figure 3c). The geometrical features of the three overlap interactions and their associated energies are collected in Table 2. We observe that, from the **B** to the **C** phase, a large molecular displacement within the Ni1−Ni1 dyad leads to a decreasing Ni1−Ni1 interaction and, hence, from a magnetic point of view, to the formation of tetrameric Ni1−Ni2−Ni2−Ni1 units, interacting more weakly with each other along the stacking direction.

The whole **A** → **B** → **C** sequence can therefore be described as the evolution from a uniform spin chain with almost negligible antiferromagnetic interactions (phase **A**) to an alternated spin chain with stronger interactions (phase **B**) and finally to a full spin localization in a structure (phase **C**) with antiferromagnetically coupled tetramers. In this latter **C** phase, we are then left with the magnetic contribution of the ferricinium cations, characterized (Figure 4) by a strong decrease of the χT product below 50 K, attributable to the Fe^{III} anisotropy.

Discussion

From the χT vs T data obtained for $[Cp_2Fe][Ni(tfadt)_2]$, two structural transitions affecting the magnetic susceptibility have been identified. The first-order character of these transitions, inferred from the hysteresis observed for both of them (>10 K), has been confirmed by DSC measurements. Note also here that the occurrence of two regions of bistability in such molecular systems is quite rare and, to our knowledge, has only be reported in a few spin crossover system where the intermediate spin state can be stabilized as in dinuclear iron(II) complexes.[28] The collection of X-ray structural data below those two first-order phase transitions represents a real *tour de force* and offers an invaluable rationale to correlate the magnetic behavior with structural changes.

The structural sequence observed here, that is, uniform chain/dimerized chain/tetramerized chain, is usually observed with *mixed valence* conducting salts such as $(TMTTF)_2X$ (Fabre salts) or $MEM(TCNQ)_2$ (MEM: methylethylmorpholinium) but not in spin chains with a full charge transfer. Indeed, in such conducting salts,[29] the uniform chain is associated with a $^1/_4$ or $^3/_4$ filled conduction band and a metallic behavior. The dimerization of the chains hence corresponds to a spin localization (or $4k_F$ transition) and transition to a semiconducting but still magnetic phase, while the tetramerization observed at lower temperatures is described as a spin-Peierls transition, since it involves a tetramerization expected from a normal Peierls transition but establishes on an insulating, already dimerized, localized phase. In the present case, the alternated chain (phase **B**) with its associated singlet ground state does not represent the real, low-temperature ground state since a tetramerized system (phase **C**) is observed. Note that this low temperature phase could have been easily overlooked since it affects only marginally the total spin susceptibility, due to the large contribution of the ferricinium and the almost diamagnetic behavior of the alternated chains at these temperatures. We believe that the driving force for this low temperature transition is essentially of structural origin and related to a lateral deformation of the stacks that cannot stand anymore the longitudinal compression experienced at the high temperature transition. It affords this tetramerized structure, with the sizable slippage between Ni1/Ni1 complexes (Figure 3c).

The second point concerns the nature of the **A** ↔ **B** transition, which looks like a spin-Peierls transition but exhibits a hysteresis normally associated with first-order transitions while the spin-Peierls one is normally a second-order transition. Indeed, the "classical" spin-Peierls transition is an intrinsic instability of spin $^1/_2$ antiferromagnetic Heisenberg chains.[30,31] Below T_{SP}, an elastic distortion of the uniform spin chain occurs, leading to a chain dimerization and two, unequal alternating exchange constants. This dimerization increases progressively as the temperature is lowered and reaches a maximum at zero temperature. It opens an energy gap between the singlet nonmagnetic ground state and the triplet excited states which stabilizes the exchange energy of the spin system. Only very few materials show a spin-Peierls transition and most often at low temperatures, such as, for example, $MEM(TCNQ)_2$ (T_{SP} = 18 K),[32] $(DMeDCNQI)_2M$ (DMeDCNQI = 2,5-dimethyldicyanoquinodiimine, M = Li, Ag),[33] $(TTF)[M(S_2C_2(CF_3)_2)]$ (M = Au, Cu),[34] $(TMTTF)_2X$ (X = PF_6, AsF_6),[35] α′-$(BEDT\text{-}TTF)_2[Ag(CN)_2]$,[29b,36] $(BCP\text{-}TTF)_2X$ (X = PF_6, AsF_6),[37] and recently biferrocene-$Ni(mnt)_2$ charge-transfer complexes.[38] On the other hand, since the pioneering work of Awaga on the magnetic bistability of 1,3,5-trithia-2,4,6-triazapentalenyl,[18] numerous 1,3,2-dithazolyl radicals have been found to exhibit first-order phase transitions accompanied by lattice dimerization.[19] In these

(28) Garcia, Y.; Grunert, C. M.; Reiman, S.; van Campenhoudt, O.; Gütlich, P. *Eur. J. Inorg. Chem.* **2006**, 3333.
(29) Jérome, D. *Chem. Rev.* **2004**, *104*, 5565 and references therein
(30) (a) Bray, J. W.; Interrante, L. V.; Jacobs, I. S.; Bonner, J. C. *Extended Linear Chain Compounds*; Plenum: New York, 1983; Vol. 3, p 353.
(31) Enoki, T.; Miyazaki, A. *Chem. Rev.* **2004**, *104*, 5449.
(32) (a) Blundell, S. J.; Pratt, F. L.; Pattenden, P. A.; Kurmoo, M.; Chow, K. H.; Takagi, S.; Jesstädt, T.; Hayes, W. *J. Phys.: Cond. Matter* **1997**, *9*, L119. (b) Obertelli, S. D.; Friend, R. H.; Talham, D. R.; Kurmoo, M.; Day, P. *J. Phys.: Cond. Matter* **1989**, *1*, 5671. (c) Huizinga, S.; Kommandeur, J.; Sawatsky, G. A.; Thole, B. T.; Kopinga, K.; de Jongh, W. J. M.; Roos, *J. Phys. Rev. B* **1979**, *19*, 4723.
(33) (a) Nakazawa, Y.; Sato, A.; Seki, M.; Saito, K.; Hiraki, K.; Takahashi, T.; Kanoda, K.; Sorai, M. *Phys. Rev. B* **2003**, *68*, 085112. (b) Meneghetti, M.; Lunardi, G.; Bozio, B.; Pecile, C. *Synth. Met.* **1991**, *41*−*43*, 1775.
(34) Jacobs, I. S.; Bray, J. W.; Hart, H. R.; Interrante, L. V.; Kasper, J. S.; Wtakins, G. D.; Prober, D. E.; Bonner, J. C. *Phys. Rev. B* **1976**, *14*, 3036.
(35) Laversanne, R.; Amiell, J.; Coulon, C.; Garrigou-Lagrange, C.; Delhaes, P. *Mol. Cryst. Liq. Cryst.* **1985**, *119*, 317.
(36) Parker, I. D.; Friend, R. H.; Kurmoo, M.; Day, P. *J. Phys.: Cond. Matter* **1989**, *1*, 5681.
(37) (a) Ducasse, L.; Coulon, C.; Chasseau, D.; Yagbasan, R.; Fabre, J.-M.; Gousmia, A. K. *Synth. Met.* **1988**, *27*, B543. (b) Liu, Q.; Ravy, S.; Pouget, J.-P.; Coulon, C.; Bourbonnais, C. *Synth. Met.* **1993**, *55*−*57*, 1840.
(38) Mochida, T.; Takazawa, K.; Matsui, H.; Takahashi, M.; Takeda, M.; Sato, M.; Nishio, Y.; Kajita, K.; Mori, H. *Inorg. Chem.* **2005**, *44*, 8628.

Table 3. Crystallographic Data for $[Cp_2Fe][Ni(tfadt)_2]$ at Different Temperatures

phase	**A** (293 K)	**B** (230 K)	**C** (120 K)
formula	$C_{18}H_{10}F_6\ FeN_2NiS_4$	$C_{18}H_{10}F_6\ FeN_2NiS_4$	$C_{18}H_{10}F_6\ FeN_2NiS_4$
fw	611.08	611.08	611.08
cryst syst	monoclinic	triclinic	triclinic
space group	*C*2/*m*	$P\bar{1}$	$P\bar{1}$
a/Å	23.039(3)	7.8764(11)	12.237(3)
b/Å	7.7428(7)	11.5708(16)	12.877(2)
c/Å	12.9602(14)	12.9460(16)	14.957(3)
α/deg	90.00	74.955(15)	77.67(2)
β/deg	99.459(13)	83.431(16)	70.47(2)
γ/deg	90.00	76.137(16)	79.62(2)
V/Å^3	2280.5(4)	1104.5(3)	2154.9(7)
Z	4	2	4
d_{calc}/Mg m^{-3}	1.780	1.837	1.884
diffract.	Stoe-IPDS	Stoe-IPDS	Stoe-IPDS
temp/K	293(2)	230(2)	120(2)
μ/mm^{-1}	1.885	1.946	1.995
θ-range/deg	2.15−24.2	1.65−25.75	1.46−25.97
meas refls	11 252	12 861	24 568
indep refls	2375	3992	7685
R_{int}	0.0486	0.0589	0.1714
$I > 2\sigma(I)$ refls	1287	2131	2984
abs corr	multiscan	gaussian	multiscan
T_{min}, T_{max}	0.540, 0.577	0.499, 0.851	0.5768, 0.7962
refined par	214	289	577
$R(F)$, $I > 2\sigma(I)$	0.0399	0.0512	0.0737
$wR(F^2)$, all	0.1162	0.1592	0.2365
$\Delta\rho$ (e Å^{-3})	+0.46, −0.36	+0.72, −0.47	+1.08, −1.36

compounds, the presence of hysteresis, hence the first-order character, was attributed to the combined effects of strong interstack interactions and electric polarization effects in the dimerized structure, which may create a potential barrier between the low- and high-temperature phases, by analogy with spin-crossover compounds. This has been followed more recently by the identification of magnetic switching in various $Ni(mnt)_2^{-\bullet}$ salts,[17,20,39] where the bistability was also attributed to the combined effects of hydrogen bonding[20] and $\pi-\pi$ interactions.[40]

In the present case, the **A** ↔ **B** transition is associated with a growing dimerization of the uniform chains of $[Ni(tfadt)_2]^{-\bullet}$ anions and an increasing magnetic coupling of the spins. It cannot be described as a spin-Peierls transition since it exhibits a first-order character with a large hysteresis and a transition enthalpy (4.8 J g^{-1}). However, its first-order character can hardly be attributed to the presence of hydrogen bonding or strong interstack interactions since, as mentioned above, the nickel dithiolene stacks are essentially isolated from each other. As this transition is also associated with the simultaneous ordering of both the Cp and CF_3 groups, disordered in the **A** phase, we postulate that the process is mainly driven by the order−disorder behavior of both CF_3 and Cp groups. These observations offer a powerful concept for the purposeful elaboration of bistable systems, by coupling an electronic transition of interest to an order−disorder transition, rather than by looking for a strengthening of intermolecular interactions. Fragments such as trifluoromethyl groups are very attractive in that respect since they are often disordered at room temperature, a consequence of the very weak polarizability of the aliphatic fluorine which limits the efficiency of van der Waals interactions in the solid state.

Experimental Section

Syntheses. $[Cp_2Fe][Ni(tfadt)_2]$: Under a nitrogen atmosphere, 4-cyano-5-trifluoromethyl-1,3-dithiole-2-one (0.6 g, 2.84 mmol) is added to a freshly prepared solution of Na (0.14 g, 6 mmol) in dry MeOH (15 mL). The mixture is stirred for 45 min, $NiCl_2(H_2O)_6$ (0.33 g, 1.42 mmol) is added, the red solution is stirred for 20 min, and $[Cp_2Fe][BF_4]$ (0.77 g, 2.8 mmol) is added. After 30 min, water (80 mL) is added affording a black precipitate which is filtered, washed with water, dried by suction, and washed with diethyl ether and pentane. The black residue is dissolved in dichloromethane and filtered. Slow evaporation of the solvent yields black plates (0.35 g, 0.57 mmol, 41%) suitable for X-ray characterization (Phase **A**). Explosive dec: 207 °C. Anal. Calcd for $C_{18}H_{10}F_6N_2S_4FeNi$: C, 35.38; H, 1.65; N, 4.58. Found: C, 35.23; H, 1.45; N, 4.57. IR (KBr) ν 2211.35 cm^{-1} (C≡N).

DSC Experiments. Differential scanning calorimetric scans were obtained with 10 mg of product sealed in an aluminum holder on a DSC 2010 CE from TAinstruments at scan rates of 10 or 5 K/min for cooling and warming scans, respectively. Transition enthalpies were estimated by using the peak integration software provided with the instrument and averaging over the cooling and warming runs. Transition entropies were estimated from the transition enthalpies, assuming a first-order transition according to the expression[41]

$$\Delta H_t = T_t\,\Delta S_t \qquad (1)$$

where ΔH_t, ΔS_t, and T_t are the transition enthalpy, entropy, and transition temperature, respectively.

X-ray Data Collection and Structure Refinements. Crystals of $[Cp_2Fe][Ni(tfadt)_2]$ were mounted at the end of a glass fiber with Aradilte glue. The temperature cycle applied to the crystals is detailed below. Crystal no. 1: at rt, data collection phase **A**; from rt at −50 K/h to 245 K, then at −1 K/h to 230 K, data collection phase **B**. Attempts to cool to lower temperatures resulted in the crystal breaking into parts. Crystal no. 2: from rt at −50 K/h to 245 K, then at −1 K/h to 230 K, unit cell control: phase **B**. From 230 K at −10 K/h to 155 K, then at −1 K/h to 120 K, data collection phase **C**.

(39) Willett, R. D.; Gomez-Garcia, C. J.; Ramakrishna, B. L.; Twamley, B. *Polyhedron* **2005**, *24*, 2232.
(40) Ni, Z.; Ren, X.; Ma, J.; Xie, J.; Ni, C.; Chen, Z.; Meng, Q. *J. Am. Chem. Soc.* **2005**, *127*, 14330.
(41) Swamy, M. J.; Marsh, D.; Ramakrishnan, M. *Biophys. J.* **1997**, *73*, 2556

Data were collected on a Stoe Imaging Plate Diffraction System (IPDS) with graphite monochromated Mo Kα radiation ($\lambda = 0.710\ 73$ Å). The crystal data are summarized in Table 3. Structures were solved by direct methods (SHELXS-97) and refined (SHELXL-97) by full matrix least-squares methods. Absorption corrections were applied for all structures. Hydrogen atoms were introduced at calculated positions (riding model), included in structure factor calculations, and not refined. Disorder models were used in the room-temperature structure of $[Cp_2Fe][Ni(tfadt)_2]$ phase **A** for one CF_3 and one Cp group. Refinement of occupation parameters led to a 50:50 distribution. This value was then fixed and not refined any more.

Magnetic Measurements. The magnetic susceptibility measurements were obtained with the use of a Quantum Design SQUID magnetometer MPMS-XL. This magnetometer works between 1.8 and 400 K for dc applied fields ranging from −7 to 7 T. Measurements were performed on finely ground crystalline samples of $[Cp_2Fe][Ni(tfadt)_2]$ (21.28 mg). *M* vs *H* measurements have been performed at 100 K to check for the presence of ferromagnetic impurities that has been found absent. The magnetic data were corrected for the sample holder and the diamagnetic contribution.

Acknowledgment. Financial support of the Ministry of Education and Research (France) to O.J. is gratefully acknowledged. R.C. thanks MAGMANet (NMP3-CT-2005-515767), the CNRS, Bordeaux 1 University, and the Conseil Régional d'Aquitaine for financial support.

Supporting Information Available: X-ray crystallographic data (CIF) for the three structures reported. This material is available free of charge via the Internet at http://pubs.acs.org.

JA064842V